Influence of Porous Structure of Non-Autoclaved Bio-Based Foamed Concrete on Mechanical Strength

Abdelrahman MOHAMAD , Fouzia KHADRAOUI * , Daniel CHATEIGNER , Mohamed BOUTOUIL

Posted Date: 6 July 2023

doi: 10.20944/preprints202307.0280.v1

Keywords: foamed concrete; porous structure; mechanical strength; bio-based concrete; hemp shiv

Article

Influence of Porous Structure of Non-Autoclaved Bio-Based Foamed Concrete on Mechanical Strength

Abdelrahman Mohamad [1], Fouzia Khadraoui [1,*], Daniel Chateigner [2] and Mohamed Boutouil [1]

[1] ComUE Normandie Université, Builders Ecole d'Ingénieurs, Builders Lab 1 Rue Pierre et Marie Curie, 14610 Epron, France
[2] CRISMAT, CNRS UMR 6508, ENSICAEN, IUT Caen, Université de Caen Normandie, Normandie Université, 6 Bd Maréchal Juin, 14050 Caen Cedex 4, France
* Correspondence: fouzia.khadraoui-mehir@builders-ingenieurs.fr

Abstract: This study investigates the influence of the porous structure, on the density and the mechanical behaviour of new foam concretes incorporating hemp shives. A total of eight batches of foam concretes were manufactured and tested, made with a protein-based foam agent, containing cement, ground granulated blast furnace slag and Metakaolin as binder and hemp shives as natural aggregate. The effect of several parameters is studied, elaboration method (direct and preformed), amount of pozzolanic additions (0% and 30%) and incorporation of hemp shives (5 and 15 vol%) on the resulting physical properties, microstructure, porous structure and mechanical behaviour of the concretes. Hemp shives incorporation results in increased concrete porosity and air bubble radius, decreased uniformity and mechanical strength, and lower cohesion with the cement matrix compared to standard concretes.

Keywords: foamed concrete; porous structure; mechanical strength; bio-based concrete; hemp shiv

1. Introduction

For their many advantages, lightweight, aerated and foamed concretes are widely used in the construction field. Foamed concrete (FC) is a mineral matrix incorporating air or gas bubbles. Generally, FC is designed to exhibit a low density ranging from 400 to 1850 kg/m^3, a very low thermal conductivity compared to usual concretes (from 0.06 to 0.66 W/mK) and a low compressive strength of about 1-30 MPa [1]. Futhermore, Foamed concrete provides other advantages, such as reduced construction costs, production of lightweight and environmentally friendly structures, sound insulation and fire resistance [2–5].

There are two mechanical processes to elaborate, foamed non-autoclaved concrete (Figure 1). On one hand, the preformed foaming method (Preformed Foam) uses an agent to generate foam before addition to the mineral mix, an adequate technique to produce foamed concrete with high porosity and stable air bubbles [6]. On the other hand the direct mixing method (By mixing) consists in generating air bubbles directly in the mineral matrix by adding and mixing the foaming agent directly into the cement paste [7]. Several studies have investigated the performance and pore structure of FC with raw material additives such as ground granulated blast furnace slag (GGBFS) and fly ash (FA), as industrial by-products and have been considered as sustainable materials in the development of an eco-friendly and sustainable concrete [8,9]. In addition, FA and GGBFS have also been used in the production of foam concrete as cement replacement materials [10,11]. Also polypropylene [12] and natural [13] fibres have been used to reinforce the foam concrete, and few studies investigated the influence of hemp shives incorporation [14].

Preprints (www.preprints.org) | NOT PEER-REVIEWED | Posted: 6 July 2023 doi:10.20944/preprints202307.0280.v1

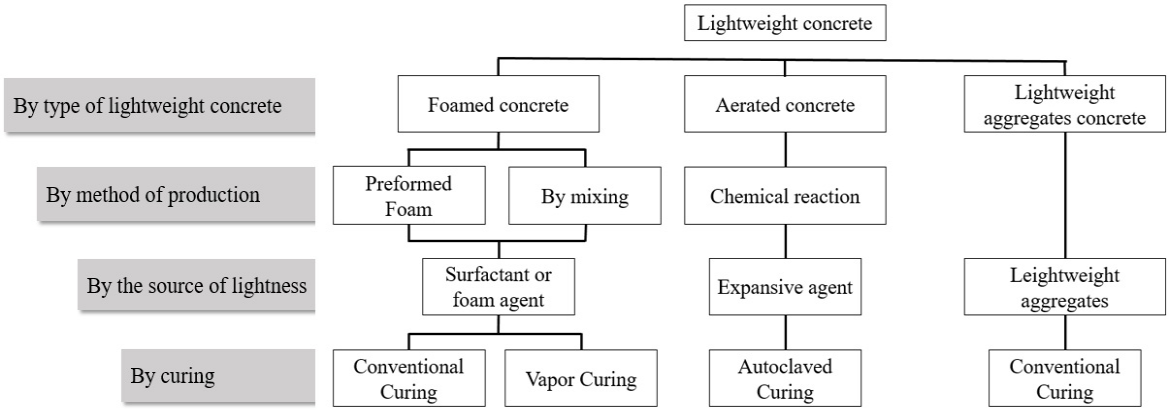

Figure 1. Flowchart of the different types of lightweight concretes.

Usually, hemp shives are used as an alternative to aggregates. For instance, Sáez-Pérez et al. [15] found that the hemp concrete can be used as construction and an insulation material. The valuable characteristics of hemp concrete are their lightweight, highly porous structure, low thermal conductivity, excellent moisture buffer capability and acoustic insulation, all allowing reduction of building energy consumption [16,17]. Also, biogenic materials are playing an increasingly important role in the composition of building materials [18].

Air-voids in the foam concrete can be characterized using few parameters like volume, radius, distribution, shape and spacing between voids [1]. The porosity and the air bubbles structure appear to condition the thermal conductivity and mechanical properties of foam concrete [19]. For instance Kearsley et al. proved on one hand that the air-void distribution is one of the most important micro properties influencing strength of foam concrete, and on the other hand that foam concrete with narrower air-void distributions exhibits higher strengths [20]. According to Visagie et al. [21], large total porosity ϕ will significantly reduce compressive strength, especially if the pores are large. Like conventional cementitious materials, foamed concrete consists of nano-pores (also called gel pores) (with a diameter < 0.01 μm), capillary or micropores (0.01 μm - 10 μm) and macro-pores (> 10 μm diameter).

The addition of GGBFS enhances mechanical strength. Moreover, a study on the air-void system of foamed concrete shows that incorporation of GGBFS leds to a high strength-to-weight ratio [22]. Other parameters affecting the strength of foam concrete are cement/sand and water/cement ratios, curing regime, sand type and its particle size distribution and type of foaming agent [23,24]. For a dry density of foamed concrete between 500 and 1000 kg/m^3, the compressive strength decreases with increasing void diameter. For densities above 1000 kg/m^3, as the air voids are widely spaced to influence the compressive strength, the composition of the concrete mix has a higher effect on the compressive strength [25].

The importance of the pore structure on the performances of foamed concretes guided us to explore in the present work the physical properties to pore structure relationship in bio-based foamed concretes, with special emphasis on pore effects on the concrete mechanical behavior. The pore structure is characterized using surface characterization techniques based on image analysis which allows to carry out the first observations of the alveolar distribution of air bubbles. The relationships between hemp shives quantity, elaboration process, pore structure and associated mechanical performances are described.

Preprints (www.preprints.org) | NOT PEER-REVIEWED | Posted: 6 July 2023 doi:10.20944/preprints202307.0280.v1

2. Materials and Methods

2.1. Raw materials

The raw materials used for producing FC are:

(i) CEM I 52.5N, which fulfils all the specifications of EN 197-1 Portland cement Type 1.
(ii) Ground Granulated Blast Furnace Slag (GGBFS), which complies with I.S EN 206-1, as by-product from iron production.
(iii) Metakaolin (MK) is obtained by flash calcination of kaolinite at approximately 700°C.
(iv) biomass consisting of 95% hemp shives (HS) and 5% hemp fibre, hemp shives being considered as renewable raw materials to reduce cost and CO_2 emissions.

A low water/binder ratio and an optimized granular density of the binder matrix would lead to a very solid cementitious matrix, constituting the interface between the air bubbles. Pozzolans are used to increase resistance to sulphate attack and durability, and to reduce CO_2 emissions due to cement and heat of hydration [26]. Therefore, GGBFS and MK are used in this study (Table 1).

Table 1. Chemical composition of binder components.

Components	CEM I	GGBFS	MK
Calcium oxide (CaO)	64.17	43	0.2
Aluminum oxide (Al_2O_3)	4.44	10.7	24.1
Silicon dioxide (SiO_2)	19.6	37.3	68.1
Ferric oxide (Fe_2O_3)	4	0.2	3.7
Sulfur trioxide (SO_3)	2.6	0.1	-
Sodium oxide (Na_2O)	0.07	0.23	0.1
Magnesium oxide (MgO)	1.25	6.5	0.2
Potassium oxide (K_2O)	0.84	0.35	0.4
Absolute density (kg/m³)	3100	2900	2500

To obtain acceptable workability of the mixture while maintaining the low W/C ratio, a superplasticizer based on polycarboxylate and modified phosphonates is incorporated in each sample to reduce the amount of water while keeping good fluidity of the fresh mixture. To produce a more stable bubble network, a commercial foaming agent is used with a foam density of about 70 kg/m³. The foaming agent limits the degree of hardening due to its retarding side effect. A setting accelerator is therefore used to support the hydration reactions of the cements, improve the stability of air bubbles in the cement matrix and rapidly develop mechanical strength. Also, in order to ease demoulding of foam concrete after hardening, a demoulding agent is used, whose composition does not contain solvents, to form an anti-adhesive film on the surface of the mould. The characteristics of the superplasticizer, accelerator, and foaming agent are given in Table 2.

Table 2. Properties of admixtures used in this study.

	Accelerator	Superplasticizer	Foam agent
Color	Yellow	brown	bright yellow
Absolute Density (g/cm³)	1.45 ± 0.01	1.055 ± 0.01	1.04 ± 0.02
Recommended weight	1-1.5 %	1-3 %	-
Chlorides content	≤ 0.1 %	≤ 0.1 %	0,001 %
pH	6 ± 1	6 ± 1	9
Dry Content (%)	61.5 % ± 2.7 %	30.5 % ± 1.5 %	30 %

2.2. Specimens elaboration

A total of eight foam concrete samples were prepared, four using the preformed and four using the direct methods.

Preprints (www.preprints.org) | NOT PEER-REVIEWED | Posted: 6 July 2023 doi:10.20944/preprints202307.0280.v1

The preformed foam method is based on the separate production of a stable aqueous foam and a mineral suspension, which are then mixed. On the one hand, the foam is produced by mixing the diluted foaming agent with water in a 1:30 ratio (by weight). On the other hand, the powdered constituents and hemp shives are first mixed dry in a mortar mixer with a capacity of about 20L, then water is added with an accelerator and superplasticizer and the mixture is stirred until a homogeneous paste is obtained. Finally, the mineral suspension is added to the foam gradually and stirred (at high speed) until the mixture becomes homogeneous.

The direct method is based on the addition of a foaming agent directly into the mineral mixture after its formation, the preparation of the mineral mixture is the same in both methods.

With both methods, the obtained concrete is fluid and foamy, then placed without any vibration in parallelepiped moulds (4 x 4 x 16 cm^3). After 48 hours curing at 20 °C, the samples are demoulded and stored in a damp room (20 °C, RH > 95 %). Six 4x4x16 samples are used to study the mechanical behaviour (in compression and flexion) at 7 and 28 days, the other three provide an analysis of the distribution of air bubbles.

Two control foam concrete formulations are used (Table 3), C100H0 and C70H0 (in CxHy, x represents the weight percentage of cement and y the wt% of cement replaced by hemp shiv). Also, in order to specify the method used, D or P are added to the sample name for "direct" and "preformed" methods respectively.

Table 3. Compositions of formulations studied.

Mixes Names	Fresh density (kg/m^3)	Composition of mixture (kg/m^3)							Wt/L
		CEM I	GGBFS	MK	HS	SP	Acc	FAG	
C100P0H0P	891	700	-	-	-	14	7	2.1	0.24
C100P0H0D	1600	1200	-	-	-	24	12	2.1	0.24
C70P30H0P	933	490	140	70	-	7	7	2.1	0.31
C70P30H0D	1589	840	240	120	-	12	12	2.1	0.31
C65P30H5P	900	455	140	70	2.2	6.7	6.7	2.1	0.32
C65P30H5D	1542	780	240	120	3.8	11.4	11.4	2.1	0.32
C55P30H5P	834	385	140	70	6.7	6.1	6.1	2.1	0.34
C55P30H5D	1227	660	240	120	11	10.3	10.31	2.1	0.34

Based on the high-water absorption capacity of the hemp particles (about 250% of the hemp mass), a competition for water occurs between hydration of the the mineral binders and water absorption of the hemp shives [43,44]. This leads to chalking of the hydraulic binders at the interface between the hemp particle and the binder [45]. Therefore, the amounts of water in the different formulations are adjusted according to the volume of hemp shiv.

2.3. Methods

The fresh density is measured in a one-litre container with a measuring error of 20 kg/m^3 according to NF EN 12350-6. Dry bulk density is measured in accordance with the NF EN 12390-1 standard by drying a group of three 4x4x16 specimens at a temperature of 60 °C until the weight is constant; the weight/volume ratio becomes the density.

According to ASTM B923, the measurement of absolute density is investigated by AccuPyc II 1340 helium pycnometer. It accurately measures the volume of the solid phase of a sample of known weight.

After 7 and 28 days, a parallelepiped specimen is broken in 2 halves by bending and the compressive strength is measured on both halves. The load velocity is 0.05 kN/sec. A universal press (IGM® 250KN press) is used to determine the compressive strength Rc and the bending strength. These tests are controlled by adapting the standards EN 679 and EN 196. The thermal conductivity at 7 and 28 days is measured by an HFM 436 Lambda flowmeter (NETZSCH) in accordance with EN 12667 standard.

Preprints (www.preprints.org) | NOT PEER-REVIEWED | Posted: 6 July 2023 doi:10.20944/preprints202307.0280.v1

The images obtained by the Keyence microscope allow a first observation of the pore structure (Figure 2). It is necessary to use an image analysis software to study the distribution of air bubbles and hemp shives. For this purpose, the ImageJ software is used first to determine the surface contribution of the hemp shives and remove it. Then, (Figure 3) the (x,y) positions of the air bubbles are determined on the sample surface, together with their perimeter, surface, small and large radius of the ellipse and sphericity, by applying several image treatment and analysis (Figure 4). However, it is sometimes difficult to differentiate between two porous structures or to extract quantitative elements to compare them; for this purpose, the use of a coal powder to fill the air bubbles is necessary.

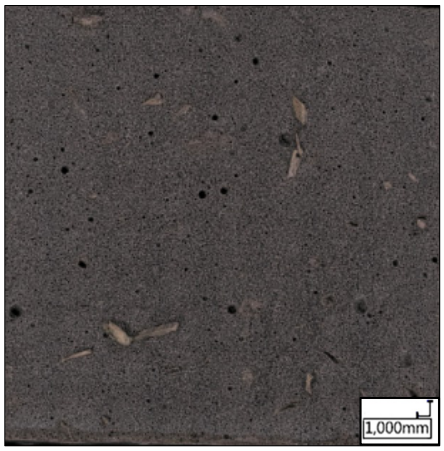

Figure 2. Raw image of the bio-based foamed concrete. Image size is 10000x10000 pixels.

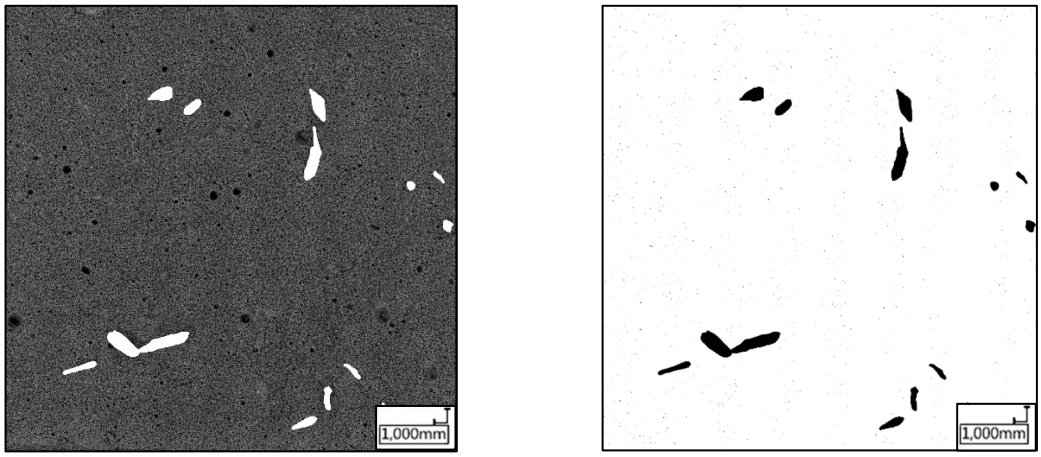

(**a**) (**b**)

Figure 3. Calculation and elimination of the amount of hemp shives. Image size is 10000x10000 pixels.

Preprints (www.preprints.org) | NOT PEER-REVIEWED | Posted: 6 July 2023 doi:10.20944/preprints202307.0280.v1

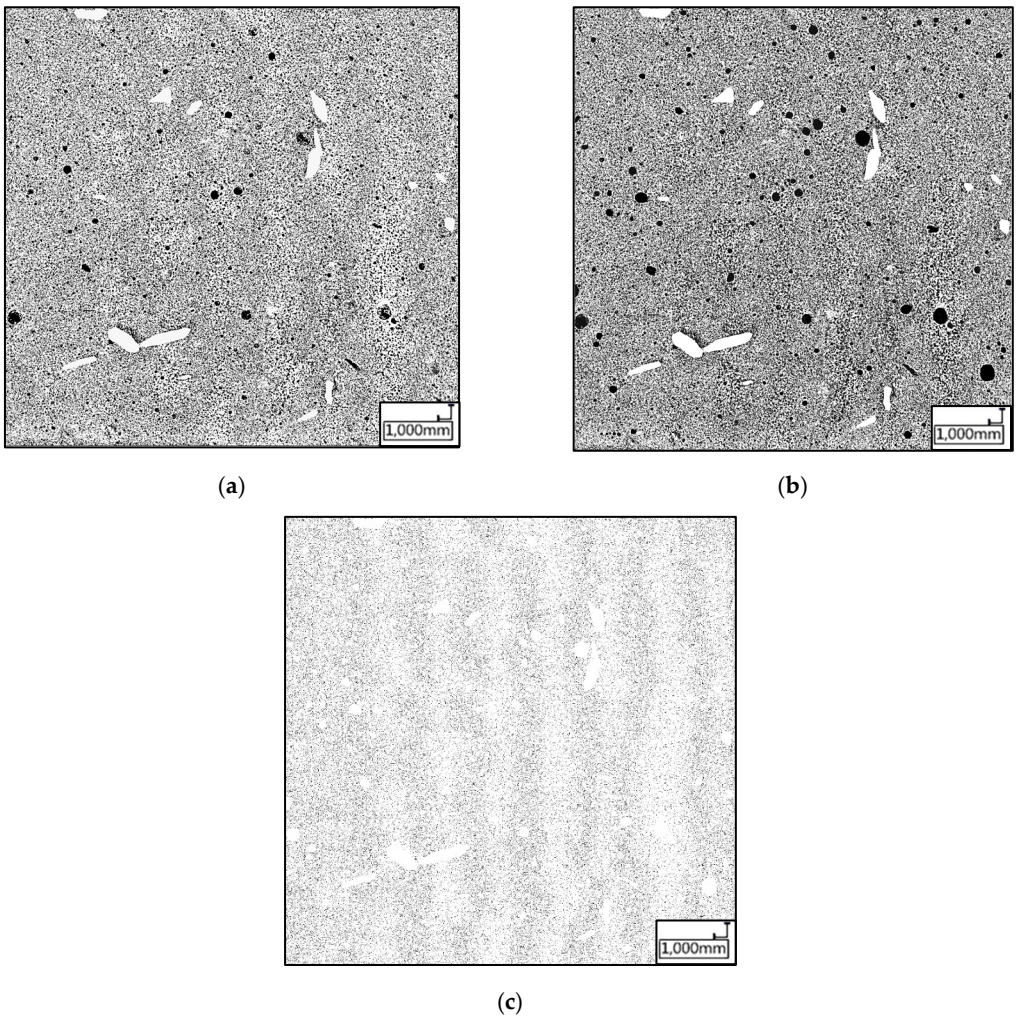

(**a**) (**b**)

(**c**)

Figure 4. Image treatment steps using Image J: (**a**) Contouring of the individual cells; (**b**) Removal of HS reflections and air bubbles detection and is coloring (black); (**c**) Edge detection analysis assuming ellipsoidal contours.

3. Results and discussion

The parameters studied in this work include the quantity of cement and its substitution ratio by hemp aggregates. The density, porosity, compressive and flexural strengths and porous structure of the different types of foamed concretes and their mutual effects are evaluated.

3.1. Physical properties

Porosity (opp. Density) is the most influential factor in the performance of foamed concrete, such as mechanical strength, thermal conductivity, water resistance and durability, and is related to the amount of foam, water, admixtures and hemp shives in the formulation. According to the NF EN 1097 standard, total porosity is obtained from the absolute density and the bulk density using the following equation:

$$\Phi = (1 - \frac{\rho_{bulk}}{\rho_{abs}}) \times 100$$

ρ_{bulk}: Bulk density (kg/m³).
ρ_{true}: Absolute density (kg/m³).

The bulk densities of the preformed samples range from 579 kg/m³ to 710 kg/m³ (Table 4) with a large total porosity from 70.7 % to 74.5 % while the samples elaborated using the direct method exhibit bulk densities in the 1092 - 1617 kg/m³ total porosity in the 32.2 - 54.6 % ranges respectively. The observed lower total porosity of foamed concretes obtained by the direct method is due to the

Preprints (www.preprints.org) | NOT PEER-REVIEWED | Posted: 6 July 2023 doi:10.20944/preprints202307.0280.v1

direct formation of air bubbles in the mineral suspension which exerts a high pressure on their surfaces [27]. Using preformed foams, air first penetrates the water to generate the foam and subsequent addition of the mineral suspension, mixing at very high rotation speed, air trapped in the foam remains in the cementitious matrix to form the foamed concrete. Obviously, many factors affect the control of air bubble production such as rotation speed, time and mixing directions, which are kept constant in this work.

Table 4. Physical properties of the biobased foamed concretes.

Sample	Days	ρ_{bulk} (kg/m³)	ρ_{True} (kg/m³)	Porosity (%)
C100H0P	7	710	2444	71.4
	28	699		
C100H0D	7	1460	2444	40.5
	28	1454		
C55H15P	7	579	2361	74.2
	28	608		
C55H15D	7	1092	2361	54.1
	28	1083		
C65H5P	7	597	2381	72.2
	28	662		
C65H5D	7	1565	2381	33.9
	28	1574		
C70H0P	7	690	2384	71.0
	28	691		
C70H0D	7	1617	2384	32.8
	28	1601		

The comparison of the density and porosity of C55H15P, C65H5P and C70H0P samples (Table 4) shows that sample porosity increases with the increase of hemp shives. This appears as a coherent behaviour since hemp shives exhibit a very low absolute density compared to cement, 140 kg/m³ and 3100 kg/m³ respectively.

As shown in Table 2, the absolute density of pozzolanic admixtures is slightly lower than that of cement, but the total density of C100H0D is lower than that of C70H0D. The explanation for this is that the direct method is relatively hard to control, depending on several parameters such as mixing time, mixing speed, quantity of surfactants, water quantity and formulation constituents [1].

For all the elaborated foams the porosity-density relationship evolves linearly (Figure 5). A linear fit of this latter indicates a very similar slope for both direct and preformed elaborated samples.

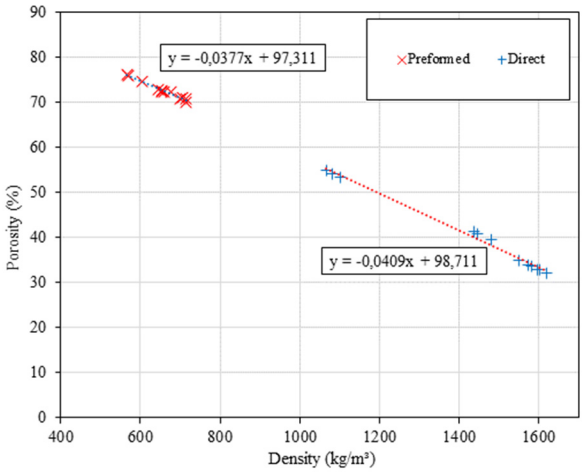

Figure 5. Porosity of all samples against bulk density.

Preprints (www.preprints.org) | NOT PEER-REVIEWED | Posted: 6 July 2023 doi:10.20944/preprints202307.0280.v1

3.2. Pore size distributions and resulting mechanical strength

We operated image analysis to evaluate the pore surface distributions of the samples. The homogeneity of the distributions was verified using measurements operated on 3 different sections for each sample (Figures 6 and 7). Whatever the measured section, the pore distributions peak for their maximum at 0.08 mm radius pores (Figure 6), corresponding to a partial area around 45-50% of the apparent total pore section.

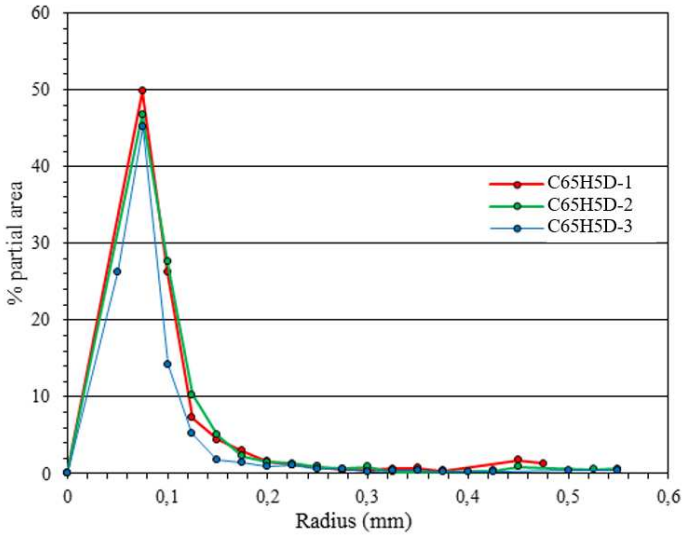

Figure 6. Pore distributions for the three sections of C65H5D illustrating the size-homogeneity of the porosity through the sample.

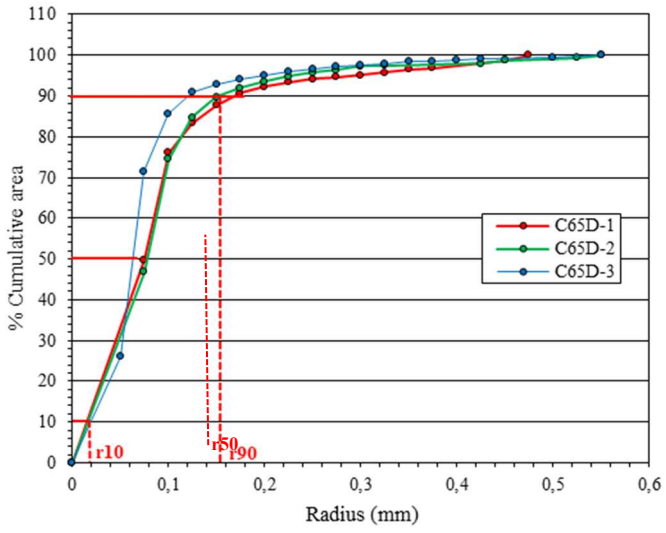

Figure 7. Cumulative pore-size distribution for the three sections of C65H5D.

3.2.1. Influence of pozzolanic additions on pore distribution

We illustrate the effects of cement replacement by pozzolanic additions (Table 5) on the pore-size distribution of BFCs, comparing one sample without pozzolan addition (C100H0) to one with 30% addition (C70H0 with 20 wt% of GGBFS and 10 wt% of MK). Each sample is elaborated using the two methods, without HS addition. From image analysis, the mean pore radius (Rm), their pore-size-distribution (PSD) and the uniformity coefficient (UC) of the samples provide a macroscopic measure of pozzolan addition effects (Table 5 and Figure 8). In the literature, pore-size distribution

Preprints (www.preprints.org) | NOT PEER-REVIEWED | Posted: 6 July 2023 doi:10.20944/preprints202307.0280.v1

is considered totally uniform if UC = r90/r10 = 1, with a decreasing homogeneity for increasing UC ratio [27].

However, in our samples, the UC parameter is a too restrictive view of the homogeneity. Indeed, while UC values (Table 5) seem to indicate weaker pore-size homogeneity using the direct method, comparing the pore size fraction distribution curves (Figure 8), one can clearly see that the direct method provides samples exhibiting much steeper step-like curves than the preformed method, pointing for a larger size homogeneity in the former. These apparently contradictory observations are explained by the large variability of UC estimation on very steep curves, and on the weakness in representing distributions using only a single number (UC). For instance, C100H0P and C70H0D samples which exhibit similar UC values but different mean pore radius (Table 5) are showing very different pore-size distributions (Figure 8a and 8b respectively).

Nevertheless, the distribution curves for samples with 30% pozzolanic additions are steeper than the ones without pozzolanic additions for both methods, and pozzolanic additions give rise to smaller UCs, both indicators pointing to more pore-size uniformity upon pozzolan additions. This larger uniformity is accompanied by a mean pore-size decrease, from 0.242 to 0.188 and 0.153 to 0.088 in the preformed and direct methods respectively. One can also observe that the mean pore-size decrease due to pozzolan addition is more efficient using the direct than using the preformed method, with Rm being 57% and 77% of their value without addition respectively.

Table 5. Uniformity Coefficient (UC) and mean pore radius (Rm) as a function of the amount of pozzolans (PZ) for the two-elaboration method.

		Preformed		Direct	
Sample	**%PZ**	**UC**	**Rm (mm)**	**UC**	**Rm (mm)**
C100H0	0	8.41	0.242	9.73	0.153
C70H0	30	5.1	0.188	8.1	0.088

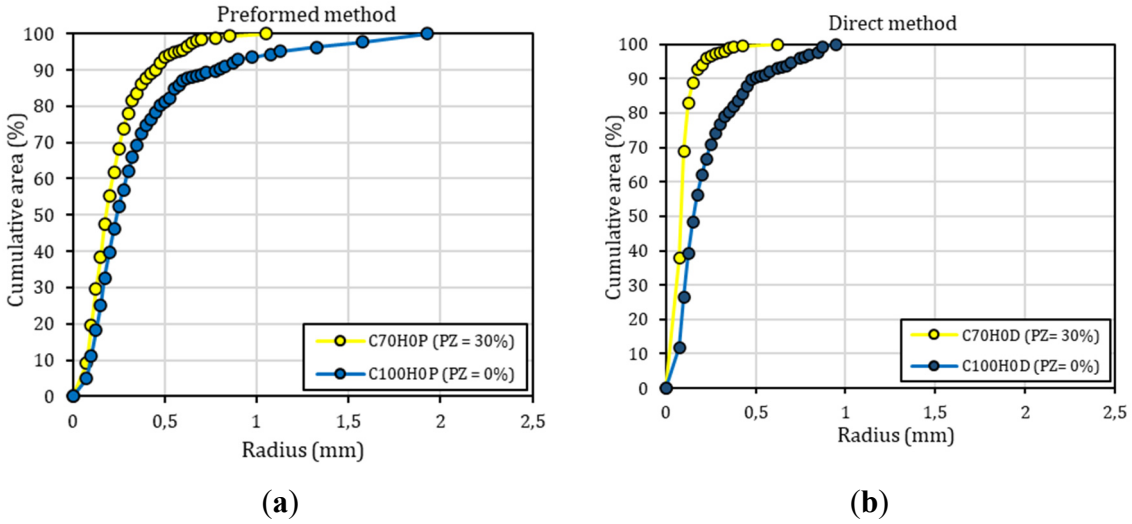

(**a**) (**b**)

Figure 8. Cumulative pore fraction versus their radius for the two pozzolan fractions: (**a**) preformed and (**b**) direct methods.

The pore-size refinement upon pozzolan additions is also visible directly from microscopic images (Figure 9, compare 9a and 9c to 9b and 9d images). The main effect of pozzolanic additions is to ensure cohesion between particles and fill voids which blocks the coalescence of pores, resulting in their smaller size and larger uniformity, also reflected in the PSD (Figure 8) as smoother curve evolutions for C70HO samples. This smoothing effect is clearly observed by the disappearance of

Preprints (www.preprints.org) | NOT PEER-REVIEWED | Posted: 6 July 2023 doi:10.20944/preprints202307.0280.v1

large pores (Figure 9c) giving rise to the angular variations of the PSD around 0.5 mm radii (Figure 8b) upon pozzolan addition (Figure 9d).

The observed PSD steepness differences between the two elaboration methods is due to the foaming capacity, the preformed method having a larger capacity to generate pores than the direct method, as seen from the more than 2 times smaller density of the formers.

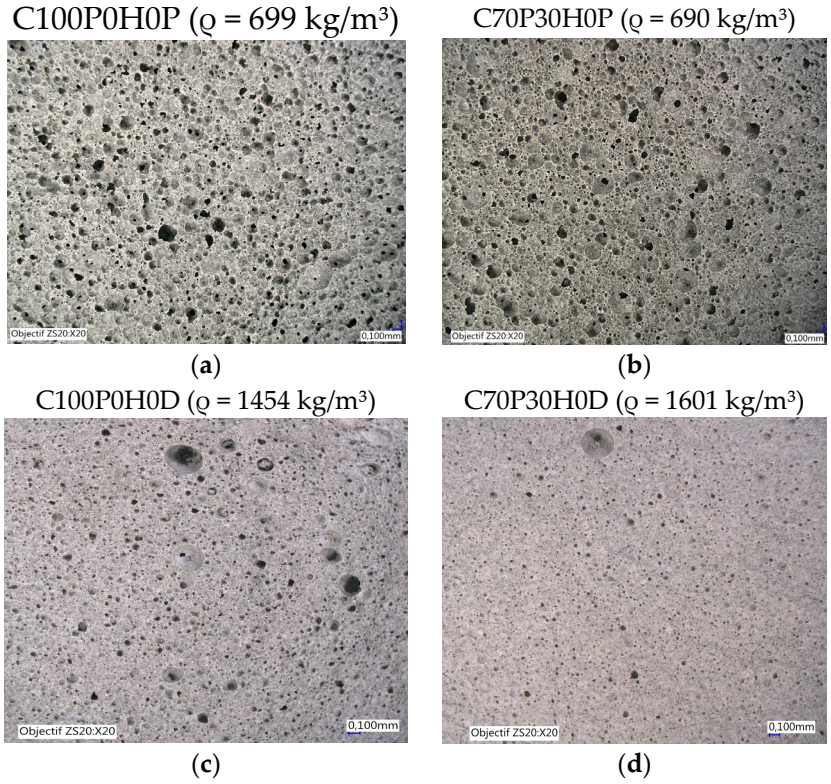

Figure 9. Microscopic images of the porous microstructures of preformed (**a**,**b**) and direct (**c**,**d**) method samples with (**b**,**d**) and without (**a**,**c**) pozzolanic additions.

3.2.2. Influence of hemp shiv on pore distributions

Hemp shives incorporation in the samples affects their density and consequently getting a more detailed picture of their porosity is of major importance.

Using the preformed method (Figure 10a), incorporation of up to 15% hemp shives in 30% pozzolan BFC's does not severely affect the distribution of pores. Only a slight tendency toward larger pore-size ranges is observed. This is reflected by an increase of both UC and Rm values of 27% and 11% respectively up to 15%HS addition (Table 6).

Table 6. Uniformity Coefficient UC and the mean radii Rm as a function of the amount of hemp shiv (HS).

		Preformed		Direct	
Mixe	**%HS**	**UC**	**Rm (mm)**	**UC**	**Rm (mm)**
C70H0	0	5.1	0.182	8.1	0.088
C65H5	5	5.79	0.219	11.33	0.063
C55H15	15	6.48	0.2	13.52	0.151

Preprints (www.preprints.org) | NOT PEER-REVIEWED | Posted: 6 July 2023 doi:10.20944/preprints202307.0280.v1

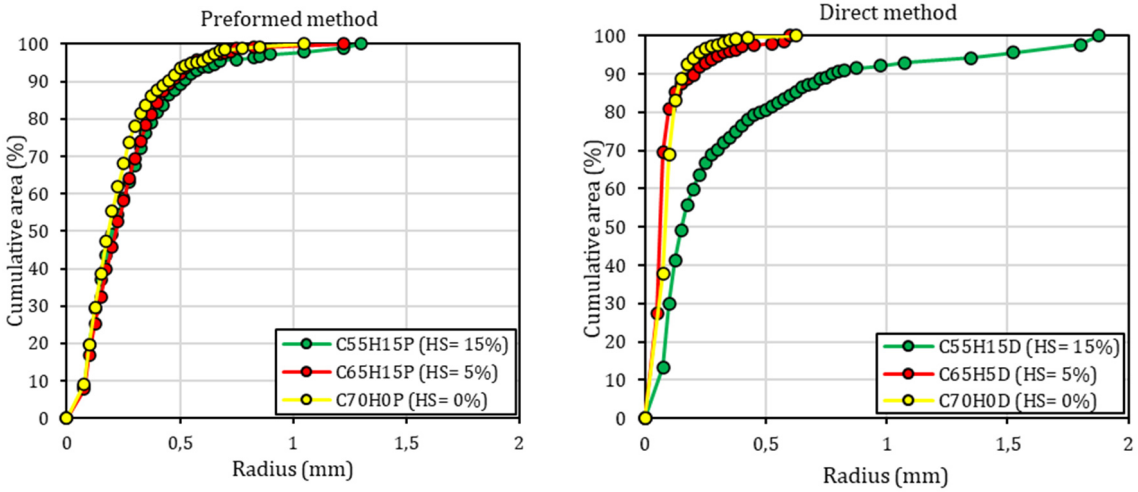

(**a**) (**b**)

Figure 10. Cumulative pore area versus radius of BFCs incorporating various amounts of hemp shiv (HS) using: (**a**) preformed method, (**b**) direct method.

Using the direct method (Figure 10b) pore distribution and mean pore radii are also only slightly modified upon hemp shiv addition up to 5%. However, for larger hemp shiv contents (HS = 15%), the pore distribution is skewed towards larger sizes, giving rise to larger UC and Rm values, this latter reaching twice the value without hemp shiv addition.

Optical microscopy images of the porous structures evidence their invariance upon hemp shiv addition using the preformed method (Figure 11). Whatever the HS content, pore sizes and distribution are constant and hemp shiv coherently integrated into the BFC matrix with no visible interface between HS and the matrix at these magnifications. Using the direct method (Figure 12), large pores are developed upon HS addition, via pore coalescence, and consequently both UC and Rm are increased by a factor of nearly 2. However in this case, contrarily to the preformed samples, a low cohesion between the hemp shives and the cement matrix are observed and result in a larger pore size distribution [31,32]. This decrease in pore size uniformity may consequently affect the mechanical resistance.

Figure 11. Microscopy images of porous structure evolution with increasing amount of hemp shiv using the preformed method.

Preprints (www.preprints.org) | NOT PEER-REVIEWED | Posted: 6 July 2023 doi:10.20944/preprints202307.0280.v1

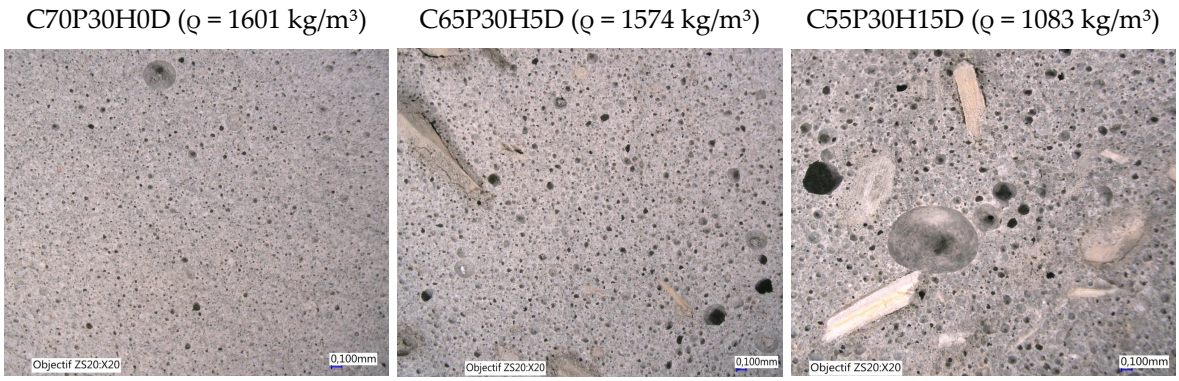

Figure 12. Microscopy images of porous structure evolution with increasing amount of hemp shiv using the direct method.

3.2.3. Influence of production process on pore distribution

Whatever HS content and pozzolanic additions (Table 7), all BFCs elaborated by the direct method exhibit finer pore distributions and mean radii.

Table 7. Uniformity Coefficient UC and the mean radii r50 as a function of production methods.

Sample	Rm (mm)	UC
C100H0P	0.242	9.73
C100H0D	0.153	8.41
C70H0P	0.182	5.1
C70H0D	0.088	8.1
C65H5P	0.219	5.73
C65H5D	0.063	11.33
C55H15P	0.2	6.48
C55H15D	0.151	13.52

These two next paragraphs are not really enlightening. The first one does not say more than what was already said in the previous, and the second concerns more the influence on mechanical strength. I would remove 3.2.3. C65H5D (Rm = 0.063 mm) and C65H5P (Rm = 0.219 mm) have the same formulation with different production methods. C65H5D foam is produced using the direct mixing method while C65H5P foam is produced using the preformed method. The direct method does not produce a light foam with such a low surfactant dosage. Additionally, for all the other foamed concrete as C70H0 and C100H0, the difference of the average radius is significant but for the C55H15D foams, the radii are more close (average radius of C55H15P is equal to 0.2 mm while for C55H15D is equal to 0.151 mm), due to the low uniformity caused by the low cohesion between the hemp shives and the cement matrix.

The foam in the preformed method is produced by mixing the surfactant and water and then combined with the mineral suspension. With the direct method, air bubbles are formed directly in the mineral suspension. The formation of air bubbles is consequently more difficult with the direct method and, as already proven in 3.1, the size of the radius affects the porosity. At higher foam volume, merging of bubbles results in wide distribution of void sizes leading to lower strength [25,28]. In addition to the air-void size and its distribution, the compressive strength of foam concrete is also be influenced by the void/paste ratio, spacing of air-voids, number (frequency) of air-voids. Because of the uniform shape (characterized by shape factor) of air-voids, its influence on strength is negligible [18,28,33]. Therefore, the preformed method achieves higher porosity, followed by lower densities and mechanical strength.

 doi:10.20944/preprints202307.0280.v1

3.3. Mechanical strength

Compressive strength of foamed concretes is largely dependent on age, constituents, porosity and density [20,34]. In our samples (Table 8), the ratio between Rc at 7 days and the one at 28 days increases from 0.54 to 0.74 for the samples elaborated using the preformed method, and from 0.79 to 0.88 for the direct method concretes. This increase is larger than for ordinary concretes for which such a ratio is usually observed around 0.65, and is mainly due to the hardening accelerator used. Moreover, this Rc7/Rc28 ratio also increases upon incorporation of HS, as seen in samples C55H15, C65H5 and C70H0, with ratio of 0.54, 0.58 and 0.69 for the preformed method and 0.79, 0.85 and 0.88 for the direct method respectively. A previous study of the effect of hemp shives on cement hardening [35] shows that the high alkalinity of cement may lead to the degradation of lignocellulosic compounds and generate by-products that prevent the setting and hardening process of hemp shives. Therefore, hemp shives delay concrete's hardening [36]. Additionally to HS incorporation, pozzolanic materials also delay the hydration process and extend the achievement of stabilization over time [26]. Therefore, the evolution of the mechanical strength of concrete foamed with pozzolanic raw materials C70H0 is larger than those without pozzolanic raw materials C100H0 (Table 5).

Table 8. Compressive and flexural strengths of all samples at 7 and 28 days.

Sample	Days	Density (kg/m³)	Rc (MPa)	Rf (MPa)
C100H0P	7	710	2.13	1.08
	28	699	2.88	1.36
C100H0D	7	1460	20.63	4.25
	28	1454	25,.32	4.48
C70H0P	7	690	2.3	1.23
	28	691	3.73	1.43
C70H0D	7	1617	27.53	6
	28	1601	31.48	6.22
C65H5P	7	597	2	0.85
	28	662	3.44	1.02
C65H5D	7	1565	24,5	4.43
	28	1574	28.67	5.41
C55H15P	7	579	1.8	0.84
	28	608	3.11	0.93
C55H15D	7	1092	7.05	2.01
	28	1083	8.88	2.2

The mechanical strength is also dependent on the uniformity of pore distributions and their mean radius. Indeed, HS addition in preformed samples, which exhibit fine radius distributions and dense interfaces between HS particles and the matrix, has only a moderate impact on the mechanical resistance, Rc's at 28 days decreasing from 3.73 MPa in C70HOP to 3.11 MPa in C5515P, and Rf's from 1.43 MPa to 0.93 MPa respectively.

But HS addition affects significantly the mechanical strengths of the direct method samples, Rc's and Rf's exhibiting a three fourth and two-third decrease respectively up to 15% HS contents. This is also coherent with the observations of section 3.2, with lower uniformities of the pore distributions for the largest amount of HS, and their weaker cohesion between the shives and the cementitious matrix giving rise to the formation of new porosity channels in this latter. As a result, the material becomes more brittle and therefore the foam concrete samples without or with 5% HS exhibit much larger strengths compared to those with 15% HS. These decreases in compressive strength have been reported by several authors on biofibre concretes [37–40]. Additionally, Chamoin [17] also found that the compressive strength of hemp concrete increases with the amount of binder in the formulation.

The large difference in compressive strengths in favour of concretes produced by the direct method is mainly an effect due to their larger density (see § 3.1). Some studies showed an exponential

Preprints (www.preprints.org) | NOT PEER-REVIEWED | Posted: 6 July 2023 doi:10.20944/preprints202307.0280.v1

evolution of the compressive strength with density [1,19], and this is also what we observe in our samples (Figure 13).

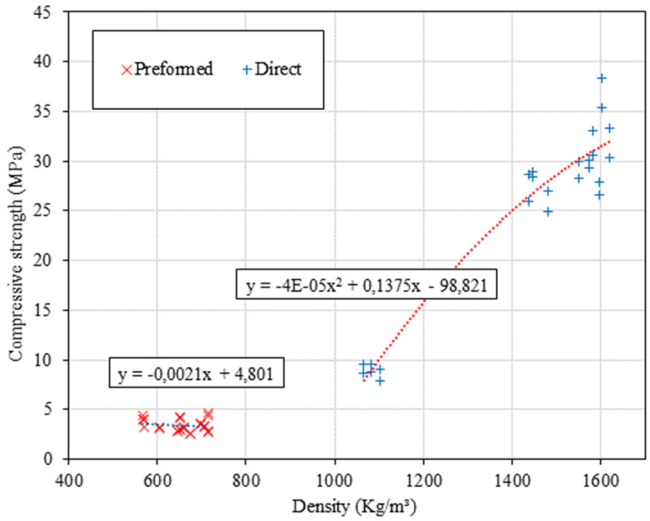

Figure 13. Compressive strength evolution with density at 28-days.

The compressive strength of C100H0D, C70H0D, C65H5D concretes is larger than 25 MPa, therefore they are considered as structural concretes.

The compressive strength behavior of our samples all lies above 2 MPa. Consequently, even the more porous samples also can be considered as semi-structural bio-based concretes. Therefore, the direct method can be used to produce structural foam concretes and the preformed method to elaborate semi-structural, ligher foam concretes.

The Rf/Rc ratio (Table 8) for the direct method is between 0.15 and 0.25 and that for the preformed method is between 0.3 and 0.45. This difference is also mainly due to the density as the Rf/Rc ratio decreases with increasing density. For instance, this ratio was observed in foamed concrete with densities lower than 1000 kg/m³ between 0.25 and 0.35 [41]. Also, in ordinary concretes it ranges usually between 0.1 and 0.2 [42]. Compared to ordinary, foamed or not, concretes, the addition of HS decreases the flexural strength less than it decreases the compressive strength, thus increasing the Rf/Rc ratio. This is the case independently of the chosen elaboration method.

Similarly as for the compressive strength, the evolution of flexure strength (Figure 14) with density in the foamed concretes exhibit a behaviour compatible with an exponential character.

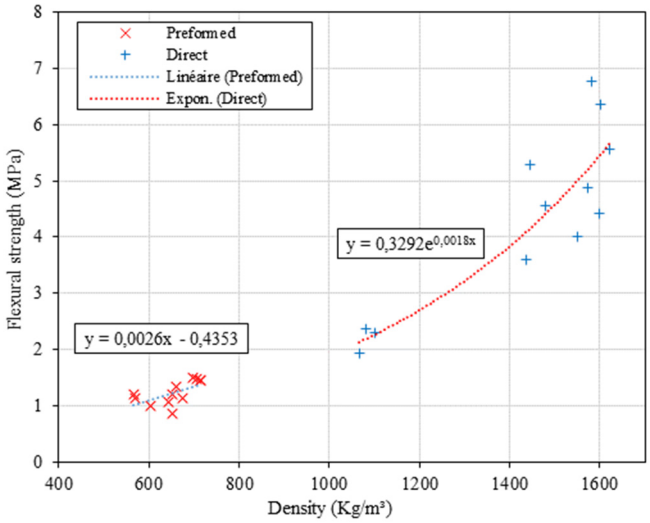

Figure 14. Flexural strength of all samples against density at 28-days.

4. Conclusion

The porous structure of non-autoclaved bio-based foamed concretes manufactured using cement, Ground Granulated Blast Furnace Slags, Metakaolin, pozzolans and hemp shives, are influencing many samples characteristics. The parameters that define the void network are correlated with the mechanical performances. We can point out the following conclusions:

- Hemp shives increase the porosity and thus decrease the density of the samples. An increase of pore mean radius is observed upon addition, which decreases pore size uniformity and correlatively the mechanical resistance.
- The amount of cement and pozzolanic materials improve slightly the uniformity of pore sizes, which increases the mechanical resistance especially at 28 days.
- The production method plays an important role in the pores formation, the preformed method is more efficient in forming foam for lightweight concretes with a density lower than 700 kg/m^3 with a compressive strength around 3.5 MPa, but the direct method gives finer pores and more uniform pore-size distributions.
- The application of a porous structure characterization technique makes it possible to establish correlations between mechanical performance and the pore structure. The mechanical strength of mineral foams depends mainly on three parameters: porosity, mineral matrix strength, distribution and size of pores. These four parameters are influenced by the formulation and production method. An analysis of the pore structure shows that a homogeneous distribution of small pores gives rise to the best mechanical performance.
- This study shows that the amount of porosity in foamed concretes is the main microstructural parameter controlling their mechanical properties.

References

1. Y.H.M. Amran, N. Farzadnia, A.A. Abang Ali, Properties and applications of foamed concrete; a review, Construction and Building Materials. 101 (2015) 990–1005. https://doi.org/10.1016/j.conbuildmat.2015.10.112.
2. K. Ramamurthy, E.K. Kunhanandan Nambiar, G. Indu Siva Ranjani, A classification of studies on properties of foam concrete, Cement and Concrete Composites. 31 (2009) 388–396. https://doi.org/10.1016/j.cemconcomp.2009.04.006.
3. E.P. Kearsley, P.J. Wainwright, Porosity and permeability of foamed concrete, Cement and Concrete Research. 31 (2001) 805–812. https://doi.org/10.1016/S0008-8846(01)00490-2.
4. N. Mohamad, W. Omar, R. Abdullah, Precast Lightweight Foamed Concrete Sandwich Panel (PLFP) Tested under Axial Load: Preliminary Results, Advanced Materials Research. 250–253 (n.d.) 1153–1162.
5. X. Zhang, Q. Yang, Y. Shi, G. Zheng, Q. Li, H. Chen, X. Cheng, Effects of different control methods on the mechanical and thermal properties of ultra-light foamed concrete, Construction and Building Materials. 262 (2020) 120082. https://doi.org/10.1016/j.conbuildmat.2020.120082.
6. J. Jiang, Z. Lu, Y. Niu, J. Li, Y. Zhang, Study on the preparation and properties of high-porosity foamed concretes based on ordinary Portland cement, Materials & Design. 92 (2016) 949–959. https://doi.org/10.1016/j.matdes.2015.12.068.
7. A. Fabien, N. Sebaibi, M. Boutouil, Effect of several parameters on non-autoclaved aerated concrete: use of recycling waste perlite, European Journal of Environmental and Civil Engineering. (2019) 1–18. https://doi.org/10.1080/19648189.2019.1647465.
8. A. Gholampour, T. Ozbakkaloglu, Performance of sustainable concretes containing very high volume Class-F fly ash and ground granulated blast furnace slag, Journal of Cleaner Production. 162 (2017) 1407–1417. https://doi.org/10.1016/j.jclepro.2017.06.087.
9. P. Nath, P.K. Sarker, Effect of GGBFS on setting, workability and early strength properties of fly ash geopolymer concrete cured in ambient condition, Construction and Building Materials. 66 (2014) 163–171. https://doi.org/10.1016/j.conbuildmat.2014.05.080.
10. L. Yang, Y. Yan, Z. Hu, Utilization of phosphogypsum for the preparation of non-autoclaved aerated concrete, Construction and Building Materials. 44 (2013) 600–606. https://doi.org/10.1016/j.conbuildmat.2013.03.070.

11. H.S. Gökçe, D. Hatungimana, K. Ramyar, Effect of fly ash and silica fume on hardened properties of foam concrete, Construction and Building Materials. 194 (2019) 1–11. https://doi.org/10.1016/j.conbuildmat.2018.11.036.
12. S. Pretot, F. Collet, C. Garnier, Life cycle assessment of a hemp concrete wall: Impact of thickness and coating, Building and Environment. 72 (2014) 223–231. https://doi.org/10.1016/j.buildenv.2013.11.010.
13. Y.H. Mugahed Amran, R. Alyousef, H. Alabduljabbar, M.H.R. Khudhair, F. Hejazi, A. Alaskar, F. Alrshoudi, A. Siddika, Performance properties of structural fibred-foamed concrete, Results in Engineering. 5 (2020) 100092. https://doi.org/10.1016/j.rineng.2019.100092.
14. N. Sebaibi, F. Khadraoui-Mehir, S. Kourtaa, M. Boutouil, Optimization of non-autoclaved aerated insulating foam using bio-based materials, Construction and Building Materials. 262 (2020) 120822. https://doi.org/10.1016/j.conbuildmat.2020.120822.
15. M.P. Sáez-Pérez, M. Brümmer, J.A. Durán-Suárez, A review of the factors affecting the properties and performance of hemp aggregate concretes, Journal of Building Engineering. 31 (2020) 101323. https://doi.org/10.1016/j.jobe.2020.101323.
16. J. De Prez, A.W. Van Vuure, J. Ivens, G. Aerts, I. Van de Voorde, Enzymatic treatment of flax for use in composites, Biotechnology Reports. 20 (2018) e00294. https://doi.org/10.1016/j.btre.2018.e00294.
17. J. Chamoin, Optimisation des propriétés (physiques, mécaniques et hydriques) de bétons de chanvre par la maîtrise de la formulation, thesis, Rennes, INSA, 2013. http://www.theses.fr/2013ISAR0016 (accessed October 11, 2018).
18. K. Ezziane, A. Bougara, A. Kadri, H. Khelafi, E. Kadri, Compressive strength of mortar containing natural pozzolan under various curing temperature, Cement and Concrete Composites. 29 (2007) 587–593. https://doi.org/10.1016/j.cemconcomp.2007.03.002.
19. G. Samson, A. PHELIPOT-MARDELE, C. Lanos, Structure porale de mousses minérales, in: Rencontres Universitaires de Génie Civil, Bayonne, France, 2015. https://hal.archives-ouvertes.fr/hal-01167751 (accessed October 11, 2018).
20. E.P. Kearsley, P.J. Wainwright, The effect of high fly ash content on the compressive strength of foamed concrete, Cement and Concrete Research. 31 (2001) 105–112. https://doi.org/10.1016/S0008-8846(00)00430-0.
21. M. Visagie, The effect of microstructure on the properties of foamed concrete, Dissertation, University of Pretoria, 2007. https://repository.up.ac.za/handle/2263/23075 (accessed July 10, 2020).
22. A.A. Hilal, N.H. Thom, A.R. Dawson, On void structure and strength of foamed concrete made without/with additives, Construction and Building Materials. 85 (2015) 157–164. https://doi.org/10.1016/j.conbuildmat.2015.03.093.
23. D. Aldridge, Introduction to foamed concrete: what, why, how?, in: Use of Foamed Concrete in Construction, Thomas Telford Publishing, 2005: pp. 1–14. https://doi.org/10.1680/uofcic.34068.0001.
24. M.S. Hamidah, I. Azmi, M.R.A. Ruslan, K. Kartini, N.M. Fadhil, Optimisation of foamed concrete mix of different sand-cement ratio and curing conditions, in: Use of Foamed Concrete in Construction, Thomas Telford Publishing, 2005: pp. 37–44. https://doi.org/10.1680/uofcic.34068.0005.
25. M. Visagie, E. Kearsley, Properties of foamed concrete as influenced by air-void parameters, Concrete/Beton. 101 (2002) 8–14.
26. 282-e-beton-ultra-leger-thermolitys.pdf, (n.d.). https://www.cerib.com/wp-content/uploads/2017/05/282-e-beton-ultra-leger-thermolitys.pdf (accessed May 13, 2019).
27. G. Samson, Synthèse et propriétés des mousses minérales, thesis, Rennes, INSA, 2015. http://www.theses.fr/2015ISAR0015 (accessed October 11, 2018).
28. E.K.K. Nambiar, K. Ramamurthy, Air-void characterisation of foam concrete, Cement and Concrete Research. 37 (2007) 221–230. https://doi.org/10.1016/j.cemconres.2006.10.009.
29. F. Batool, V. Bindiganavile, Air-void size distribution of cement based foam and its effect on thermal conductivity, Construction and Building Materials. 149 (2017) 17–28. https://doi.org/10.1016/j.conbuildmat.2017.05.114.
30. A.A. Hilal, N.H. Thom, A.R. Dawson, On entrained pore size distribution of foamed concrete, Construction and Building Materials. 75 (2015) 227–233. https://doi.org/10.1016/j.conbuildmat.2014.09.117.

31. Y. Diquelou, E. Gourlay, L. Arnaud, B. Kurek, Impact of hemp shiv on cement setting and hardening: Influence of the extracted components from the aggregates and study of the interfaces with the inorganic matrix, Cement and Concrete Composites. 55 (2015) 112–121. https://doi.org/10.1016/j.cemconcomp.2014.09.004.
32. L. Arnaud, E. Gourlay, Experimental study of parameters influencing mechanical properties of hemp concretes, Construction and Building Materials. 28 (2012) 50–56. https://doi.org/10.1016/j.conbuildmat.2011.07.052.
33. T.-H. Wee, D.S. Babu, T. Tamilselvan, H.-S. Lim, Air-void system of foamed concrete and its effect on mechanical properties, ACI Materials Journal. 103 (2006) 45–52.
34. E. Kearsley, D. Mostert, Designing mix composition of foamed concrete with high fly ash contents, Proceedings of the International Conference on the Use of Foamed Concrete in Construction. (2005) 29–36.
35. Y. Diquélou, E. Gourlay, L. Arnaud, B. Kurek, Influence of binder characteristics on the setting and hardening of hemp lightweight concrete, Construction and Building Materials. 112 (2016) 506–517. https://doi.org/10.1016/j.conbuildmat.2016.02.138.
36. G. Balčiūnas, I. Pundienė, L. Lekūnaitė-Lukošiūnė, S. Vėjelis, A. Korjakins, Impact of hemp shives aggregate mineralization on physical–mechanical properties and structure of composite with cementitious binding material, Industrial Crops and Products. 77 (2015) 724–734. https://doi.org/10.1016/j.indcrop.2015.09.011.
37. A. Kriker, G. Debicki, A. Bali, M.M. Khenfer, M. Chabannet, Mechanical properties of date palm fibres and concrete reinforced with date palm fibres in hot-dry climate, Cement and Concrete Composites. 27 (2005) 554–564. https://doi.org/10.1016/j.cemconcomp.2004.09.015.
38. C. Sawsen, K. Fouzia, B. Mohamed, G. Moussa, Optimizing the formulation of flax fiber-reinforced cement composites, Construction and Building Materials. 54 (2014) 659–664. https://doi.org/10.1016/j.conbuildmat.2013.12.038.
39. J. Page, F. Khadraoui, M. BOUTOUIL, Multi-physical properties of a structural concrete incorporating short flax fibers, Construction and Building Materials. 140 (2017) 344–353. https://doi.org/10.1016/j.conbuildmat.2017.02.124.
40. C. Sawsen, K. Fouzia, B. Mohamed, G. Moussa, Effect of flax fibers treatments on the rheological and the mechanical behavior of a cement composite, Construction and Building Materials. 79 (2015) 229–235. https://doi.org/10.1016/j.conbuildmat.2014.12.091.
41. R.C. Valore, Jr, Cellular Concretes Part 2 Physical Properties, JP. 50 (1954) 817–836. https://doi.org/10.14359/11795.
42. E. Namsone, G. Šahmenko, A. Korjakins, Durability Properties of High-Performance Foamed Concrete, Procedia Engineering. 172 (2017) 760–767. https://doi.org/10.1016/j.proeng.2017.02.120.
43. L. Arnaud (2008). Synthèse des connaissances sur les bétons et mortiers de chanvre.
44. T. T. Nguyen (2010). Contribution à l'étude de la formulation et du procédé de fabrication d'éléments de construction en béton de chanvre. Thèse de doctorant. Université de Bretagne – SUD
45. V.Cerezo (2005). Propriétés mécaniques, thermiques et acoustiques d'un matériau à base de particules végétales : Approche expérimentale et modélisation théorique. Thèse de doctorant de l'ENTPE